Published for SISSA by Springer

Received: *August 15, 2023*
Accepted: *September 25, 2023*
Published: *October 5, 2023*

Next-to-leading order electroweak corrections to $gg \to HH$ and $gg \to gH$ in the large-m_t limit

Joshua Davies,[a] **Kay Schönwald,**[b] **Matthias Steinhauser**[c] **and Hantian Zhang**[c]

[a] *Department of Physics and Astronomy, University of Sussex, Brighton BN1 9QH, U.K.*
[b] *Physik-Institut, Universität Zürich, Winterthurerstrasse 190, 8057 Zürich, Switzerland*
[c] *Institut für Theoretische Teilchenphysik, Karlsruhe Institute of Technology (KIT), Wolfgang-Gaede Strasse 1, 76128 Karlsruhe, Germany*

E-mail: j.o.davies@sussex.ac.uk, kay.schoenwald@physik.uzh.ch, matthias.steinhauser@kit.edu, hantian.zhang@kit.edu

Abstract: We compute two-loop electroweak corrections to Higgs boson pair and Higgs plus jet production, taking into account all sectors of the Standard Model. All diagrams with virtual top quarks are computed in an expansion for large top quark mass up to order $1/m_t^8$ or more. We present analytic results for the form factors and discuss the convergence properties. For the process $gg \to gH$ we also consider QCD corrections in the large-m_t limit.

Keywords: Higgs Production, Higher Order Electroweak Calculations, Higher-Order Perturbative Calculations

ArXiv ePrint: 2308.01355

https://doi.org/10.1007/JHEP10(2023)033

JHEP10(2023)033

Contents

JHEP10(2023)033

1 Introduction

Higgs boson pair production is a crucial process to obtain deeper insight into the symmetry breaking mechanism of the Standard Model (SM). For this reason, it is one of the most important processes studied in detail at the Large Hadron Collider at CERN and similarly at its High Luminosity upgrade which will begin operation within this decade. The main SM production mechanism for Higgs boson pairs is via gluon-gluon fusion and a number of higher-order corrections have been computed, mainly in the context of QCD. As far as electroweak corrections are concerned comparatively very little is known. First steps have been taken in refs. [1, 2]. In ref. [1] the two-loop box diagrams have been considered where a Higgs boson is exchanged between the massive top quarks. It has been shown that a deep expansion in the high-energy limit leads to results for the form factors which are valid in a large part of the phase space. In ref. [2] top-quark Yukawa corrections have been considered, partly in the infinite top quark mass limit. Electroweak corrections proportional to the Higgs self-couplings have been considered in ref. [3] using a numerical approach. In the present work we compute the complete NLO electroweak corrections as an expansion in the large top quark mass limit, including sub-leading terms up to $1/m_t^{10}$. The corresponding corrections in the case of QCD have been computed in refs. [4–6].

A similarly important process at the LHC is the production of a Higgs boson in association with a jet. As for Higgs boson pair production the dominant production channel is gluon-gluon fusion, with the partonic process $gg \to gH$. NLO QCD corrections have been considered in a number of works: in the large-m_t limit [7], in the high-energy limit [8–10] and numerically, including exact dependence on m_t [11–13]. NNLO corrections have even been computed in the infinite top quark mass limit [14–18]. NLO electroweak corrections via massless bottom quark loops have been computed in ref. [19], and the corrections induced by a trilinear Higgs coupling in the large top mass limit have been recently calculated in ref. [20]. In this work we compute, for the first time, the full NLO electroweak corrections involving virtual top quark loops. We consider all sectors of the Standard Model and perform an expansion for large m_t up to order $1/m_t^8$. Furthermore, we provide analytic results for the NLO QCD corrections, again expanded up to $1/m_t^8$. These expressions will be of interest for cross checks of numerical results and for the construction of approximation formulae involving expansions in different limits.

Calculations in the electroweak sector of the Standard Model are in general much more complicated than in the strong sector since many different mass scales are involved. For the case of QCD corrections it has been shown (see, e.g., refs. [21–23]) that precise approximations can be obtained by combining expansions performed in different regions of the phase space. This motivates developing these techniques beyond QCD to the electroweak sector of the Standard Model. In this work we take a first step in this direction by considering the region in which the top quark mass is larger than all other kinematic invariants. While the radius of convergence of such an expansion is limited only to small values of the centre-of-mass energy, the results will serve as benchmarks for cross checks of other expansions or for numerical results.

This paper is organized as follows: in the next section we define the form factors which describe the two processes considered, and the technical details needed for our calculation are presented in section 3. In particular, we describe the asymptotic expansion and our renormalization procedure. Section 4 contains our results for Higgs boson pair production and section 5 is dedicated to the electroweak corrections to $gg \to gH$. The QCD corrections to $gg \to gH$ are discussed in section 6. In all cases we study the influence of the higher-order $1/m_t$ terms on the form factors and provide our complete analytic expressions in the ancillary files of this paper [24]. A brief summary of our findings is provided in section 7.

2 Form factors for $gg \to HH$ and $gg \to gH$

2.1 $gg \to HH$

The amplitude for the process

$$g(q_1)g(q_2) \to H(q_3)H(q_4) \tag{2.1}$$

JHEP10(2023)033

can be decomposed into two Lorentz structures $A_1^{\mu\nu}$ and $A_2^{\mu\nu}$ which we define as

$$\begin{aligned} A_1^{\mu\nu} &= g^{\mu\nu} - \frac{1}{q_{12}} q_1^\nu q_2^\mu \,, \\ A_2^{\mu\nu} &= g^{\mu\nu} + \frac{1}{p_T^2 q_{12}} \left(q_{33} q_1^\nu q_2^\mu - 2 q_{23} q_1^\nu q_3^\mu - 2 q_{13} q_3^\nu q_2^\mu + 2 q_{12} q_3^\mu q_3^\nu \right) . \end{aligned} \tag{2.2}$$

Here $q_{ij} = q_i \cdot q_j$ with $q_1^2 = q_2^2 = 0$ and $q_3^2 = q_4^2 = m_H^2$. p_T is the transverse momentum of the final-state Higgs bosons, given by

$$p_T^2 = \frac{u\,t - m_H^4}{s} \,, \tag{2.3}$$

with the Mandelstam variables

$$s = (q_1 + q_2)^2 \,, \qquad t = (q_1 + q_3)^2 \,, \qquad u = (q_1 + q_4)^2 \,. \tag{2.4}$$

Using these definitions we introduce the form factors F_1 and F_2 as

$$\mathcal{M}^{ab} = \varepsilon_{1,\mu} \varepsilon_{2,\nu} \mathcal{M}^{\mu\nu,ab} \;=\; \varepsilon_{1,\mu} \varepsilon_{2,\nu} \delta^{ab} X_0^{\text{ggHH}} s \left(F_1 A_1^{\mu\nu} + F_2 A_2^{\mu\nu} \right) \,, \tag{2.5}$$

where a, b are adjoint colour indices, $X_0^{\text{ggHH}} = G_F \alpha_s(\mu) T_F / (2\sqrt{2}\pi)$, $T_F = 1/2$, G_F is Fermi's constant and $\alpha_s(\mu)$ is the strong coupling constant evaluated at the renormalization scale μ. We decompose the functions F_1 and F_2 introduced in eq. (2.5) into "triangle" and "box" form factors. F_1 has contributions with zero, one and two s-channel Higgs boson propagators whereas F_2 only has box contributions. Thus we write

$$\begin{aligned} F_1 &= \frac{3 m_H^2}{s - m_H^2} \left(F_{\text{tri}} + \frac{m_H^2}{s - m_H^2} \tilde{F}_{\text{tri}} \right) + F_{\text{box1}} \,, \\ F_2 &= F_{\text{box2}} \,. \end{aligned} \tag{2.6}$$

In order to obtain this decomposition it is important to re-write the factors of s which occur in the numerators during the calculation using $s/(s - m_H^2) = 1 + m_H^2/(s - m_H^2)$. Note that at two loops F_{tri} is not the same as the form factor for single Higgs boson production (as is the case for QCD corrections), since loop corrections to the HHH vertex also enter here.

We define the perturbative expansion of the form factors as

$$F = F^{(0)} + \frac{\alpha_s(\mu)}{\pi} F^{(1,0)} + \frac{\alpha}{\pi} F^{(0,1)} + \cdots \,, \tag{2.7}$$

where α is the fine structure constant and the ellipses indicate higher-order QCD and electroweak corrections.

In section 4 we discuss the results for the squared matrix element constructed from the form factors F_{tri}, $\tilde{F}_{\text{tri}}$, F_{box1} and F_{box2}. Analytic results for the leading-order form factors ($F_{\text{tri}}^{(0)}$, $F_{\text{box1}}^{(0)}$ and $F_{\text{box2}}^{(0)}$) are available from [25, 26]. Two-loop corrections to $F_{\text{box1}}^{(0,1)}$ and $F_{\text{box2}}^{(0,1)}$ originating from the exchange of a virtual Higgs boson have been computed in ref. [1] in the high-energy limit.

In figure 1 we show sample one- and two-loop diagrams contributing to $gg \to HH$. At two-loop order we have:

JHEP10(2023)033

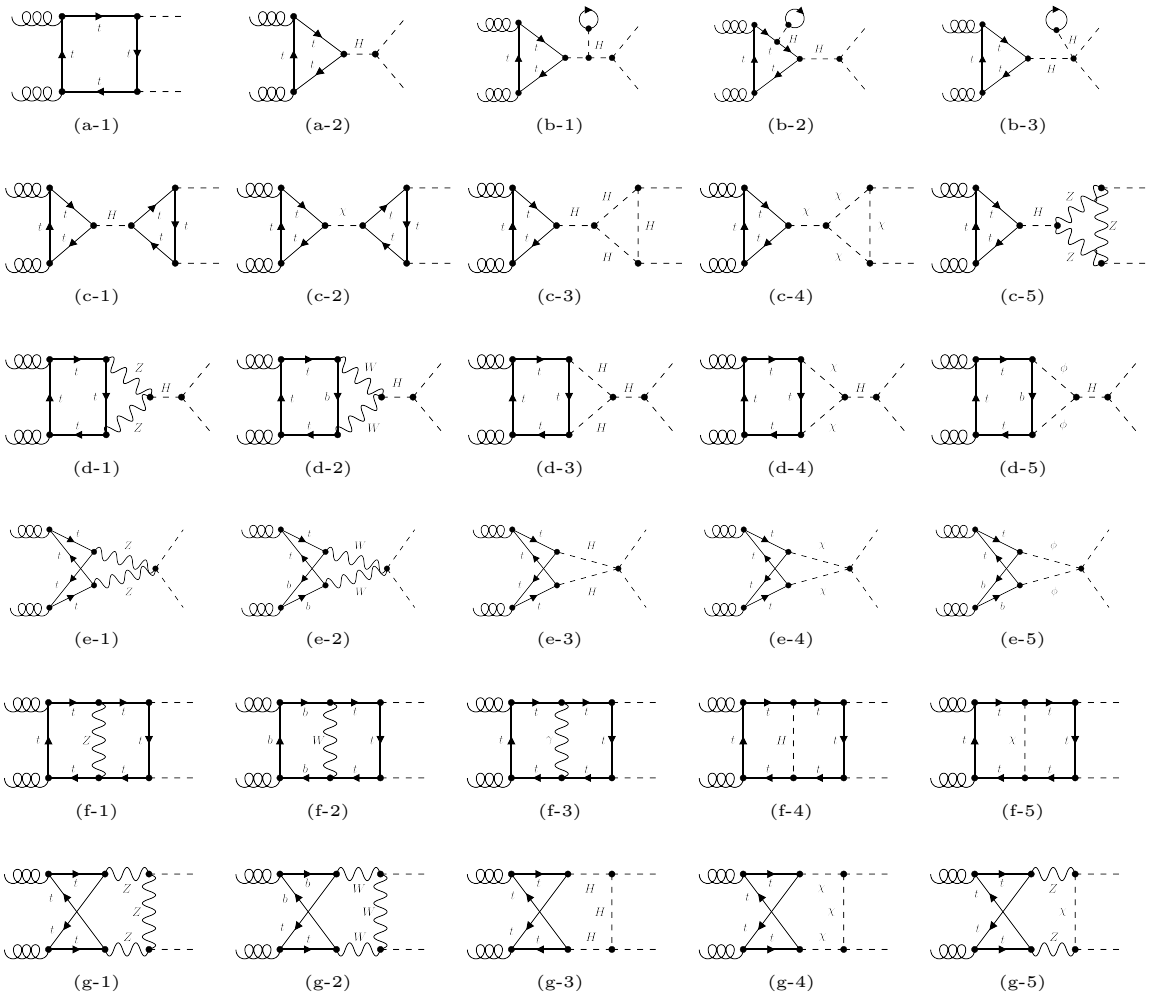

Figure 1. One- and two-loop Feynman diagrams contributing to $gg \to HH$. Dashed, solid, wavy and curly lines correspond to scalar particles, fermions, electroweak gauge bosons and gluons, respectively.

- one-particle irreducible box and triangle diagrams,
- one-particle reducible diagrams with a one-loop correction to the HHH vertex or a one-loop self-energy correction to the Higgs propagator of a one-loop $gg \to H \to HH$ diagram,
- one-loop tadpole corrections to one-loop diagrams.

At two-loop order there are also contributions without top quarks which are not suppressed by small Yukawa couplings. In these contributions the gluons couple to light quarks and the connection to the final-state Higgs bosons is mediated via Z bosons. An example is given by diagram (g-1) in figure 1 if a light quark runs in the fermion loop. In our expansion these contributions formally contribute to the m_t^0 term, however in this work we do not compute such diagrams; they can be computed following the approach of ref. [19].

JHEP10(2023)033

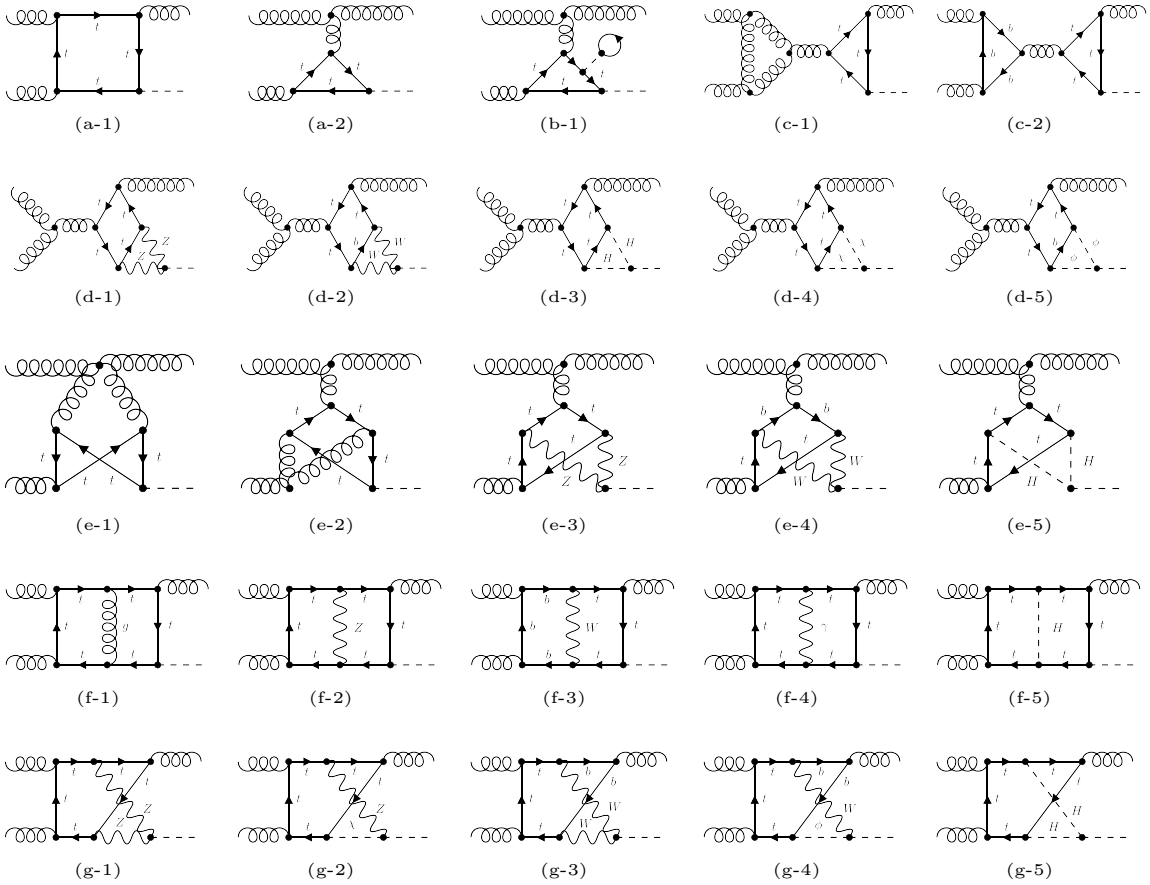

Figure 2. One- and two-loop Feynman diagrams contributing to $gg \to gH$. Dashed, solid, wavy and curly line correspond to scalar particles, fermions, electroweak gauge bosons and gluons, respectively. Diagrams are also shown which contribute to the NLO QCD corrections.

2.2 $gg \to gH$

The amplitude for the process

$$g(q_1)g(q_2) \to g(q_3)H(q_4) \tag{2.8}$$

can be decomposed into four physical Lorentz structures [8][1]

$$\begin{aligned} A_1^{\mu\nu\rho} &= g^{\mu\nu}q_2^\rho\,, & A_2^{\mu\nu\rho} &= g^{\mu\rho}q_1^\nu\,, \\ A_3^{\mu\nu\rho} &= g^{\nu\rho}q_3^\mu\,, & A_4^{\mu\nu\rho} &= \frac{1}{s}q_3^\mu q_1^\nu q_2^\rho\,. \end{aligned} \tag{2.9}$$

The corresponding four form factors $F_1, \ldots, F_4$ are defined through

$$\mathcal{M}^{abc} = f^{abc} X_0^{\text{gggH}} \varepsilon_{1,\mu}\varepsilon_{2,\nu}\varepsilon_{3,\rho} \sum_{i=1}^{4} F_i A_i^{\mu\nu\rho}\,, \tag{2.10}$$

[1]We note that $A_4^{\mu\nu\rho}$ differs from ref. [8] by the factor of $1/s$, which we introduce such that all four form factors are dimensionless.

JHEP10(2023)033

where c is the adjoint colour index of the final-state gluon, X_0^{gggH} is given by

$$X_0^{\text{gggH}} = 2^{1/4}\sqrt{4\pi\alpha_s(\mu)G_F}\,\frac{\alpha_s(\mu)}{4\pi} \tag{2.11}$$

and the perturbative expansions of the form factors are defined as in (2.7). The Mandelstam variables are defined as in eq. (2.4); the only difference with respect to $gg \to HH$ is that here $q_3^2 = 0$ and $p_T^2 = u\,t/s$. Sample Feynman diagrams for $gg \to gH$ are given in figure 2. The classification is similar to $gg \to HH$, we again include all one-particle reducible and all tadpole contributions. Note that for the QCD corrections, we also include the one-loop self-energy corrections to the gluon propagators and the one-loop vertex corrections to the triple-gluon vertex of the one-loop diagrams. The corrections to the quartic-gluon vertex do not appear at the two-loop order of this process.

3 Technical setup

3.1 Asymptotic expansion of the two-loop amplitudes

For the generation of the $gg \to HH$ and $gg \to gH$ diagrams and the corresponding amplitudes we use `qgraf` [27]. As input we use the Lagrangian file of the full Standard Model shipped with `tapir` [28], which is derived from the Feynman rules of `UFO` [29]. `tapir` translates the `qgraf` output to `FORM` [30] notation and generates further auxiliary files which are useful for the manipulation of the amplitudes. The large-m_t expansion is realized with the help of `exp` [31, 32] which generates the corresponding subdiagrams and maps them to various integral families.[2]

We apply the large-m_t limit as

$$m_t^2 \gg s, t, m_W^2, m_Z^2, m_H^2\,, \tag{3.1}$$

where no additional hierarchy is assumed among the scales on the right-hand side. This leads to the following integral families:

- one- and two-loop one-scale vacuum integrals,
- one-loop massless triangle integrals where two external lines are massless,
- massive vertex integrals where for one external leg we have $(q_1+q_2)^2 = s$ and for the other two legs we have $q_3^2 = q_4^2 = m_H^2$ (for $gg \to HH$) or $q_3^2 = 0$ and $q_4^2 = m_H^2$ (for $gg \to gH$),
- for the QCD corrections to $gg \to gH$ we also need massless one-loop box families with one external mass $q_4^2 = m_H^2$; explicit analytic results can be found in ref. [34].

Our `FORM`-based setup automatically performs a reduction of arbitrary members of each family to master integrals, which are well known in the literature (see, e.g., refs. [35, 36]). The tadpole integrals are computed by `MATAD` [37] and the remaining integral families are

[2] See also ref. [33] for a recent discussion of the expansion of integrals contributing to $H \to ggg$ in the large-m_t limit.

JHEP10(2023)033

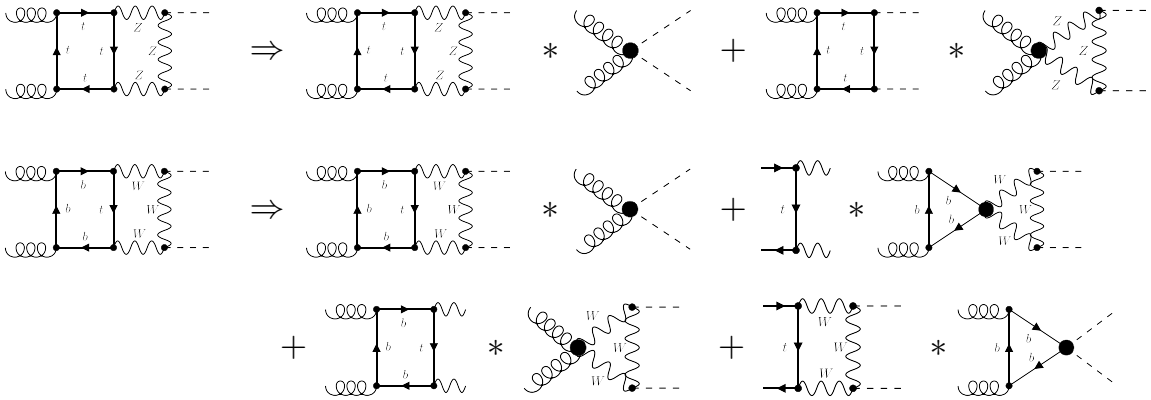

Figure 3. Asymptotic expansion of two sample Feynman diagrams. The subgraphs left of the stars have to be expanded in the small quantities, i.e., masses, external momenta or loop momenta of the co-subgraphs, which are to the right of the stars.

reduced by IBP reduction rules derived by `LiteRed` [38] which have been implemented in `FORM`. Furthermore all of our reduction routines can deal with tensor integrals, avoiding the need to construct additional projection operators. In figure 3 we show how the various integral families appear due to the asymptotic expansion in the large-m_t limit. In the Feynman gauge we have performed an expansion of the form factors up to order $1/m_t^{10}$ ($1/m_t^8$) for $gg \to HH$ ($gg \to gH$).

In order to check our calculation, we also introduce general gauge parameters ξ_Z, ξ_W and ξ_γ for the Z and W bosons and the photon. From the technical point of view ξ_γ does not introduce any additional complexity since no new mass scale is introduced. It drops out after summing all bare two-loop diagrams. This is not the case for ξ_Z and ξ_W since they appear in combination with gauge boson masses in the gauge boson and Goldstone propagators. Furthermore, ξ_Z and ξ_W only drop out after renormalization. For this check we assume

$$m_t^2 \gg \xi_W m_W^2, \xi_Z m_Z^2 \gg s, t, m_W^2, m_Z^2, m_H^2 \,, \tag{3.2}$$

and perform an expansion which includes terms up to order $1/m_t^4$, $1/(\xi_W m_W^2)^2$, $1/(\xi_Z m_Z^2)^2$, $1/(m_t^2 \xi_W m_W^2)$, $1/(m_t^2 \xi_Z m_Z^2)$ and $1/(\xi_W m_W^2 \xi_Z m_Z^2)$. To check the cancellation of ξ_Z and ξ_W we have to consider the combination of the bare two-loop diagrams and the counterterm contribution from the wave function of the external Higgs boson (see also below), which also depends on ξ_W and ξ_Z.[3] It is a welcome and non-trivial check of our calculation that up to this expansion depth, ξ_W and ξ_Z drop out of the $gg \to HH$ and $gg \to gH$ amplitudes.

3.2 Renormalization

In the following we concentrate on the electroweak sector; for the discussion of the renormalization and the treatment of the infra-red divergences which occur for the NLO QCD corrections to $gg \to gH$ we refer to section 6.

[3]Note that the counterterm contributions of the (physical) parameters are independent of the gauge parameters.

JHEP10(2023)033

For the renormalization we follow the standard procedure as outlined, e.g., in refs. [39, 40]. We express our one-loop amplitudes for the form factors in terms of the parameters

$$e, m_W, m_Z, m_t, m_H, \tag{3.3}$$

where $e = \sqrt{4\pi\alpha}$, and introduce one-loop on-shell counterterms (see, e.g. eqs. (143), (153) and (421) of ref. [40]). Furthermore, we have to renormalize the wave function of the external Higgs boson, which we also perform in the on-shell scheme (see eq. (144) of ref. [40]).

We consistently include tadpole contributions in all parts of our calculation (in the two-loop $gg \to HH$ and $gg \to gH$ amplitudes, and the gauge boson and fermion two-point functions needed for the counterterms). This guarantees that the top quark mass counterterm is gauge-parameter independent. This prescription is equivalent to the so-called *Fleischer-Jegerlehner tadpole scheme* [41].[4]

For the numerical evaluation of the form factors we transform our results into the so-called G_μ scheme where the Fermi constant G_F and the gauge boson masses m_Z and m_W are the input parameters, and the fine structure constant α and the weak mixing angle θ_W are derived quantities. (see, e.g., section 5.1.1 of ref. [40]). In this scheme it is convenient to express the final result in terms of the variable

$$x_t = \frac{G_F m_t^2}{8\sqrt{2}\pi^2}\,. \tag{3.4}$$

Although we have computed the exact top quark mass dependence of all counterterm contributions it is convenient to expand them in $1/m_t$ and combine the individual terms with the expanded bare two-loop amplitude. We do not expand the (finite) quantity Δr, which performs the transformation from the α to the G_μ scheme, in the large-m_t limit but retain its exact dependence on m_t.

Note that the NLO electroweak corrections do not produce infra-red divergences. Thus, already after renormalization we obtain the finite results for the form factors. This is not the case for the NLO QCD corrections to $gg \to gH$; the infra-red subtraction necessary to produce a finite result is discussed in section 6. Let us also mention that our NLO electroweak form factors do not have an explicit dependence on the renormalization scale since all parameters are renormalized in the on-shell scheme.

4 Results for $gg \to HH$

4.1 Analytic results

It is instructive to begin by discussing the leading contributions in the large-m_t expansion, of order m_t^4 and m_t^2, which are present in $F_{\text{tri}}^{(0,1)}$ and $F_{\text{box1}}^{(0,1)}$. Our results for the two-loop form factors read

$$\begin{aligned}
\frac{\alpha}{\pi} F_{\text{tri}}^{(0,1)} &= \frac{4}{3} \times x_t \left(\frac{136}{15} - \frac{16 m_t^2}{m_H^2} \right) + \mathcal{O}\left(m_t^0\right)\,, \\
\frac{\alpha}{\pi} F_{\text{box1}}^{(0,1)} &= -\frac{4}{3} \times \frac{4 x_t}{5} + \mathcal{O}\left(m_t^0\right)\,.
\end{aligned} \tag{4.1}$$

[4] For a recent detailed discussion on the various tadpole renormalization schemes we refer to ref. [42].

JHEP10(2023)033

For reference, we also provide the large-m_t limit of the leading-order form factors which are given by

$$F_{\text{tri}}^{(0)} = \frac{4}{3} + \mathcal{O}\left(1/m_t^2\right) ,$$
$$F_{\text{box1}}^{(0)} = -\frac{4}{3} + \mathcal{O}\left(1/m_t^2\right) . \tag{4.2}$$

Results for F_{tri} and F_{box1} have also been presented in ref. [2], in which leading m_t^2 corrections to the ggH and $ggHH$ vertices at two-loop order are taken into account using an effective-theory approach, while one-particle reducible diagrams have been computed with full m_t dependence. Furthermore, all one- and two-particle reducible diagrams involving Yukawa couplings have been considered. After extracting the m_t^4 and m_t^2 terms we find agreement with our results. To make this comparison it is important to consider subleading terms in the expansion of the LO form factors which are factored out in ref. [2] and contain exact m_t dependence.

Using the asymptotic expansion described in section 3.1 we have obtained expansion terms up to order $1/m_t^{10}$. Up to order $1/m_t^4$ we have performed the calculation for general gauge parameters and we have verified that they drop out from the renormalized results. The higher-order $1/m_t$ terms have been computed only in the Feynman gauge. The analytic expressions for the form factors can be obtained from [24].

In our analytic expressions we observe poles of the form $1/(s-4m_H^2)^k$ where $k>0$ is larger for the higher-order $1/m_t$ terms. The origin of these terms are massive one-loop triangle (co-)subgraphs, such as the one on the first row of figure 3 with external squared momenta s, m_H^2 and m_H^2. The expansion of the subgraph leads to numerators in the triangle diagram and the $1/(s-4m_H^2)$ terms result from the subsequent reduction to master integrals. We note that the poles are spurious; for each $1/m_t$ term the limit $s \to 4m_H^2$ exists.

We also point out that the m_t^0 term presented here is not complete, since it should also receive contributions from diagrams without top quarks, for e.g., the first diagram in figure 3 where the top quarks are replaced by light quarks. We do not compute such diagrams in this paper. They can be computed following the approach of, e.g., ref. [19] where similar contributions to $gg \to gH$ have been considered, or with the help of expansions as proposed, e.g. in ref. [1].

4.2 Numeric results

For the numerical evaluation of our form factors we adopt the G_μ scheme and use the following input values

$$m_t = 172 \text{ GeV}, \qquad m_H = 125 \text{ GeV},$$
$$m_W = 80 \text{ GeV}, \qquad m_Z = 91 \text{ GeV}. \tag{4.3}$$

Furthermore, we express the form factors in terms of s and p_T and introduce the parameter

$$\rho_{p_T} = \frac{p_T}{\sqrt{s}} . \tag{4.4}$$

JHEP10(2023)033

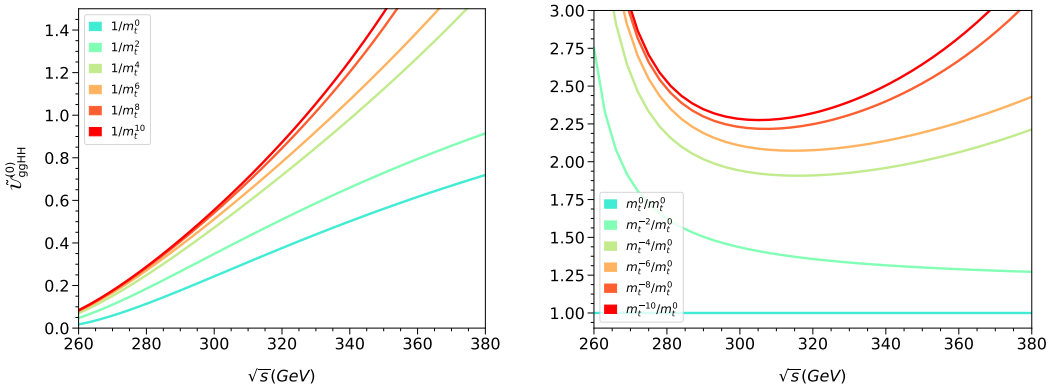

Figure 4. $\tilde{\mathcal{U}}^{(0)}_{\text{ggHH}}$ plotted as a function of $\sqrt{s}$. Results are shown up to order $1/m_t^{10}$. The panel on the right shows the result normalized to the m_t^0 expansion term.

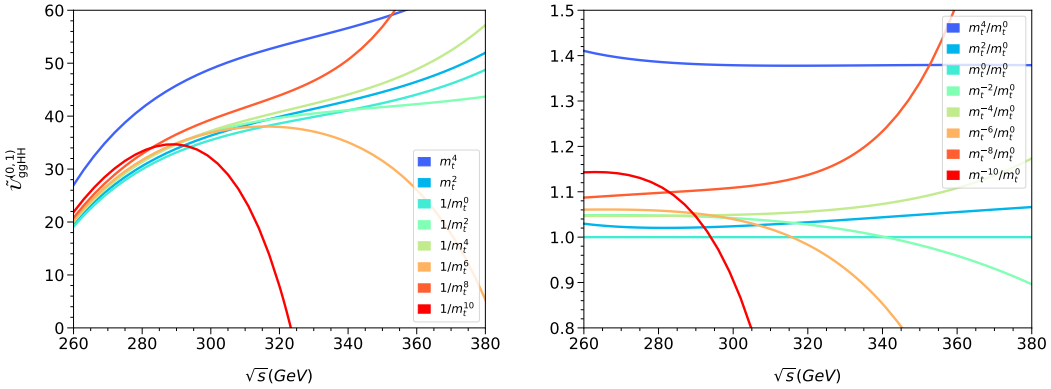

Figure 5. $\tilde{\mathcal{U}}^{(0,1)}_{\text{ggHH}}$ as a function of $\sqrt{s}$. The panel on the right shows the result normalized to the m_t^0 expansion term.

In the following we choose $\rho_{p_T} = 0.1$ and discuss results for the squared matrix element

$$\mathcal{U}_{\text{ggHH}} \equiv \frac{1}{8^2}\sum_{\text{col}}\frac{1}{2^2}\sum_{\text{pol}}|\mathcal{M}^{ab}|^2 = \frac{1}{16}\left(X_0^{\text{ggHH}}s\right)^2\left(|F_1|^2+|F_2|^2\right) = \frac{1}{16}\left(X_0^{\text{ggHH}}s\right)^2\tilde{\mathcal{U}}_{\text{ggHH}}\,. \tag{4.5}$$

For the numerical evaluation of the massive two- and three-point functions we use the program `Package-X` [43].

For reference, in figure 4 we show the LO contribution to $\tilde{\mathcal{U}}_{\text{ggHH}}$ as a function of $\sqrt{s}$. Below the top quark threshold the expansion converges well, however it converges more slowly as $\sqrt{s}$ gets closer to $2m_t$.

In figure 5 we show the NLO quantity $\tilde{\mathcal{U}}^{(0,1)}_{\text{ggHH}}$ as a function of $\sqrt{s}$. The curves include increasing expansion depths starting from the leading term proportional to m_t^4 (which originates from $F_{\text{tri}}^{(0,1)}$) up to $1/m_t^{10}$. For the $\sqrt{s}$ axis we choose values from the Higgs pair production threshold at $2m_H = 250\,\text{GeV}$ up to $\sqrt{s} = 380\,\text{GeV}$. Note that convergence of the expansion is not expected beyond the top quark pair production threshold at $2m_t =$

JHEP10(2023)033

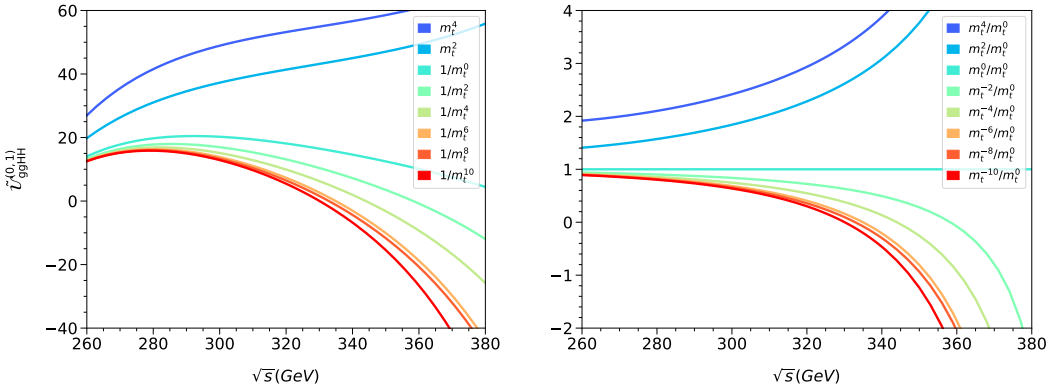

Figure 6. $\tilde{\mathcal{U}}^{(0,1)}_{\text{ggHH}}$ without contributions involving a cut at $\sqrt{s} = m_t + m_W$, see text for details. The panel on the right shows the result normalized to the m_t^0 expansion term.

344 GeV. Below this value we observe, at first sight, a reasonable convergence. Below $\sqrt{s} \approx 300\,\text{GeV}$ a significant shift is obtained from the constant contribution proportional to m_t^0 and higher order $1/m_t$ terms are small up to $1/m_t^8$. However, the $1/m_t^{10}$ contribution again provides a sizeable shift, which is clearly visible on the right panel which shows the ratio with respect to the m_t^0 contribution.

This behaviour is due to diagrams with a closed quark loop which contains both top and bottom quarks, see, e.g., the second diagram in figure 3. Such diagrams contain cuts through a top quark and W boson and thus the large-m_t expansion is expected to break down above $\sqrt{s} = m_t + m_W \approx 250\,\text{GeV}$. Diagrams with such a cut contribute to both F_1 and F_2. To demonstrate this, in figure 6 we show the results for $\tilde{\mathcal{U}}^{(0,1)}_{\text{ggHH}}$ where we set all diagrams containing a bottom quark to zero in the finite parts.[5] We indeed observe that after removing these contributions the large-m_t expansion converges as expected up to the threshold at $\sqrt{s} = 2m_t$. We note that the two-loop diagrams have further cuts where no top quark is involved at $\sqrt{s} = 2m_W, 2m_Z, 2m_H$. In our approach all of these are taken into account exactly, so they do not affect the convergence of the large-m_t expansion.

In view of the above discussion the validity of the leading m_t terms (see section 4.1 and ref. [2]), and indeed of the deeper large-m_t expansion, for a description of the electroweak corrections to $gg \to HH$ is questionable. More insight will be provided in a future publication which considers the small-t expansion of these diagrams in the style of ref. [23].

5 Results for $gg \to gH$: electroweak corrections

In this section we consider the electroweak corrections to $gg \to gH$. The QCD corrections are presented in section 6. For the input values for numerical evaluation we adopt the values given in eq. (4.3).

In order to study the convergence of the expansion in $1/m_t$ we consider the squared matrix element since the individual form factors show a divergent behaviour for $s \to m_H^2$

[5] The $1/\epsilon$ poles parts are required in order to obtain finite expressions after renormalization.

JHEP10(2023)033

which is due to contributions where a gluon is present in the t or u channel. In principle one could further decompose the form factors to make this dependence explicit, however, we prefer to consider

$$\begin{aligned}
\mathcal{U}_{\text{gggH}} &\equiv \frac{1}{8^2}\sum_{\text{col}}\frac{1}{2^2}\sum_{\text{pol}}|\mathcal{M}^{abc}|^2 \\
&= \frac{3}{32}\left(X_0^{\text{gggH}}\right)^2\left\{s\left[\frac{2F_1F_1^\star u}{t}+\frac{2F_2F_2^\star t}{u}+F_2F_1^\star+F_1F_2^\star\right]\right. \\
&\qquad +\left[F_4\left(F_3^\star+F_4^\star\right)+F_3\left(2F_3^\star+F_4^\star\right)\right]\frac{t\,u}{s} \\
&\qquad +\left[\left(F_3+F_4\right)F_2^\star+F_2\left(F_3^\star+F_4^\star\right)\right]t \\
&\qquad \left.+\left[\left(F_3+F_4\right)F_1^\star+F_1\left(F_3^\star+F_4^\star\right)\right]u\right\} \\
&= \frac{3}{32}\left(X_0^{\text{gggH}}\right)^2 s\,\tilde{\mathcal{U}}_{\text{gggH}}\,,
\end{aligned} \tag{5.1}$$

where $F_i^\star$ denotes the complex-conjugate form factors. After inserting the perturbative expansion from eq. (2.7) we obtain the LO and NLO contributions to $\mathcal{U}_{\text{gggH}}$, which converge for $s \to m_H^2$.

We start with the discussion of the LO corrections. In figure 7 we show $\tilde{\mathcal{U}}^{(0)}_{\text{gggH}}$, for $\rho_{p_T} = 0.1$, as a function of $\sqrt{s}$. The right panel shows the ratio with respect to the leading expansion term. We observe very good convergence below $\sqrt{s} = 2m_t$ and can safely assume that we reproduce the exact result every time two successive expansion terms overlap. In fact, below $\sqrt{s} \approx 250\,\text{GeV}$ only the first three terms lead to visible shifts and below $\sqrt{s} \approx 300\,\text{GeV}$ the curve which includes $1/m_t^8$ terms (which is the order we have available at two loops) provides a good approximation. The inclusion of $1/m_t^{14}$ terms extends the convergence region even further. The one-loop form factors enter the construction of $\tilde{\mathcal{U}}^{(0,1)}_{\text{gggH}}$; due to their excellent convergence it is safe to use the expansion, including terms to $1/m_t^{14}$, and avoid implementing the exact, analytic leading-order expression.

NLO results for $\tilde{\mathcal{U}}_{\text{gggH}}$ in the G_μ scheme are shown in figure 8, again for $\rho_{p_T} = 0.1$. As expected, we observe good convergence below the top quark threshold. In particular below $\sqrt{s} \approx 300\,\text{GeV}$ the higher order $1/m_t$ terms become smaller and smaller and the approximation which includes $1/m_t^8$ terms agrees well with the $1/m_t^6$ approximation. From the right panel we observe that the $\{1/m_t^2, 1/m_t^4, 1/m_t^6\}$ terms lead an almost s-independent shift of about $\{80\%, 20\%, 10\%\}$ and the $1/m_t^8$ term provides only a shift at the few-percent level.

We have compared our one-loop form factors to ref. [20] and find agreement up to $1/m_t^{14}$. We also compare with the subset of NLO contributions induced by the trilinear Higgs boson coupling considered in ref. [20], by extracting the corresponding pieces from our bare two-loop form factors. We have compared up to $1/m_t^2$ and find agreement.

Our result provides solid predictions for the energy range $m_H \leq \sqrt{s} \lesssim 300\,\text{GeV}$ and will thus serve as an important cross check for future (analytic) calculations in different kinematic limits or of numerical evaluations.

JHEP10(2023)033

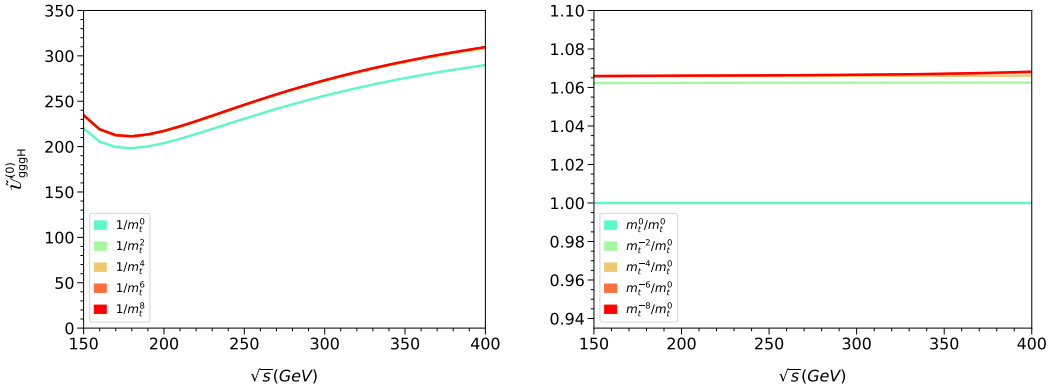

Figure 7. Left: $\tilde{\mathcal{U}}^{(0)}_{\text{gggH}}$ as a function of $\sqrt{s}$. Right: ratio with respect to the m_t^0 expansion term. The various colours correspond to the inclusion of different expansion terms.

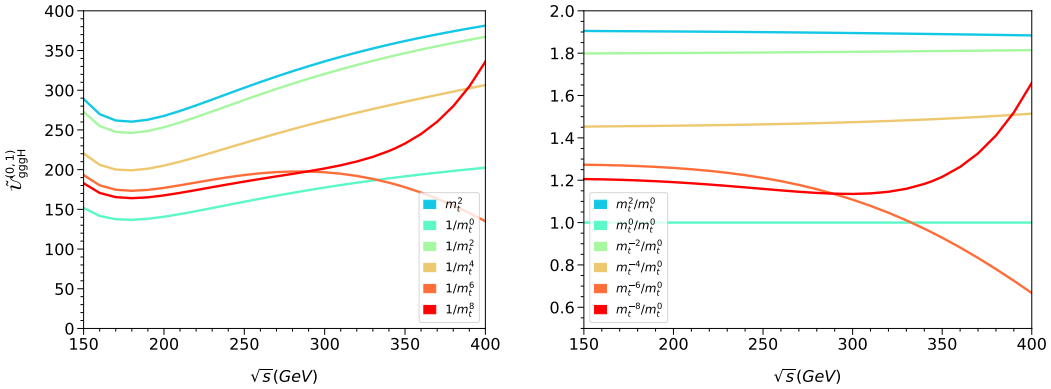

Figure 8. $\tilde{\mathcal{U}}^{(0,1)}_{\text{gggH}}$ as a function of $\sqrt{s}$. The ratio with respect to the m_t^0 expansion term is shown in the right panel.

6 NLO QCD corrections to $gg \to gH$ in the large-m_t limit

A finite expression for the NLO virtual QCD corrections to $gg \to gH$ is obtained after introducing counterterms for the ultra-violet poles and subtracting the infra-red divergences. We first renormalize the strong coupling constant in the $\overline{\text{MS}}$ scheme with six active flavours. The top quark mass and gluon wave functions are renormalized in the on-shell scheme.[6] Afterwards we express the form factors in terms of $\alpha_s^{(5)}(\mu)$, with five active flavours. Finite form factors are then obtained via the subtraction ($i = 1, 2, 3, 4$)

$$F_{i,\text{fin}}^{(1,0)} = F_{i,\text{ren}}^{(1,0)} - \frac{1}{2} I_g^{(1)} F_i^{(0)} \tag{6.1}$$

[6]The transition from the on-shell to the $\overline{\text{MS}}$ quark mass is straightforward.

JHEP10(2023)033

where $F^{(1,0)}_{i,\text{ren}}$ are the ultra-violet renormalized form factors. The quantity $I^{(1)}_g$ on the right-hand side of eq. (6.1) is given by [44]

$$I^{(1)}_g = -\frac{e^{\epsilon\gamma_E}}{2\Gamma(1-\epsilon)}\left(\frac{C_A}{\epsilon^2}+\frac{2\beta_0}{\epsilon}\right)\left[\left(\frac{\mu^2}{-s-i\delta}\right)^{\epsilon}+\left(\frac{\mu^2}{-t}\right)^{\epsilon}+\left(\frac{\mu^2}{-u}\right)^{\epsilon}\right], \tag{6.2}$$

with $\beta_0 = 11C_A/12 - T_F\, n_l/3$, where $T_F = 1/2$, $C_A = n_c$ and n_l is the number of massless quarks.

For illustration we present the one- and two-loop expressions for the form factors $F^{(0)}_1$ and $F^{(1,0)}_{1,\text{fin}}$ to the expansion order $1/m_t^2$ and m_t^0, respectively. Deeper expansions can be found in the supplementary material [24] of this paper. At one-loop order we have

$$F^{(0)}_1 = \frac{(s+t)\,(m_h^2-t)}{3su}\left[-4+\frac{1}{m_t^2}\left(\frac{7m_h^4(s+t)-tm_h^2(10s+7t)+3st(s+t)}{30(s+t)\,(t-m_h^2)}\right)\right], \tag{6.3}$$

and the two-loop expression is given by

$$\begin{aligned}
F^{(1,0)}_{1,\text{fin}} = \frac{(s+t)(m_h^2-t)}{3su}\Bigg(&-\frac{3}{2n_c}+n_c\Bigg\{2\text{Li}_2\left(1-\frac{s}{m_h^2}\right)-2\text{Li}_2\left(\frac{t}{m_h^2}\right)-2\text{Li}_2\left(\frac{u}{m_h^2}\right)\\
&+\frac{m_h^2(21s+23t)-23t(s+t)}{6(s+t)(t-m_h^2)}+\log^2\left(\frac{s}{m_h^2}\right)+\log^2\left(-\frac{t}{m_h^2}\right)\\
&+2i\pi\log\left(-\frac{t}{m_h^2}\right)-\left[2\log\left(-\frac{t}{m_h^2}\right)+2i\pi\right]\log\left(1-\frac{t}{m_h^2}\right)+\log^2\left(-\frac{u}{m_h^2}\right)\\
&+2i\pi\log\left(-\frac{u}{m_h^2}\right)-\left[2\log\left(-\frac{u}{m_h^2}\right)+2i\pi\right]\log\left(1-\frac{u}{m_h^2}\right)-\log^2\left(\frac{\mu^2}{s}\right)\\
&+\log\left(\frac{\mu^2}{s}\right)\left[\log\left(-\frac{\mu^2}{t}\right)+\log\left(-\frac{\mu^2}{u}\right)-\frac{11}{6}-2i\pi\right]\\
&-\log^2\left(-\frac{\mu^2}{t}\right)+\log\left(-\frac{\mu^2}{t}\right)\left[\log\left(-\frac{\mu^2}{u}\right)-\frac{11}{6}+i\pi\right]\\
&-\log^2\left(-\frac{\mu^2}{u}\right)-\left[\frac{11}{6}-i\pi\right]\log\left(-\frac{\mu^2}{u}\right)-\frac{5\pi^2}{6}-\frac{11i\pi}{6}\Bigg\}+\log\left(\frac{\mu^2}{m_t^2}\right)\\
&+n_l\left\{\frac{tu}{3(s+t)(m_h^2-t)}+\frac{1}{3}\log\left(\frac{\mu^2}{s}\right)+\frac{1}{3}\log\left(-\frac{\mu^2}{t}\right)+\frac{1}{3}\log\left(-\frac{\mu^2}{u}\right)+\frac{i\pi}{3}\right\}\Bigg),
\end{aligned} \tag{6.4}$$

where $n_c = 3$ and Li_2 is the dilogarithm.

In figure 9 we show the NLO QCD corrections to $\mathcal{U}_{\text{gggH}}$ for $\rho_{p_T} = 0.1$ as a function of $\sqrt{s}$. We observe a rapid convergence, even beyond the top quark threshold (although the expansion is not expected to produce the correct result in this region). In fact, only the $1/m_t^2$ terms lead to a shift of a few percent; the higher-order expansion terms are much smaller. This behaviour can be explained by the dominance of the diagrams involving ggH triangle contributions and the suppression of the box-type Feynman diagrams.

7 Conclusions

In this work we consider the gluon-fusion induced processes $gg \to HH$ and $gg \to gH$ and compute complete NLO electroweak corrections in the large top quark mass limit and

JHEP10(2023)033

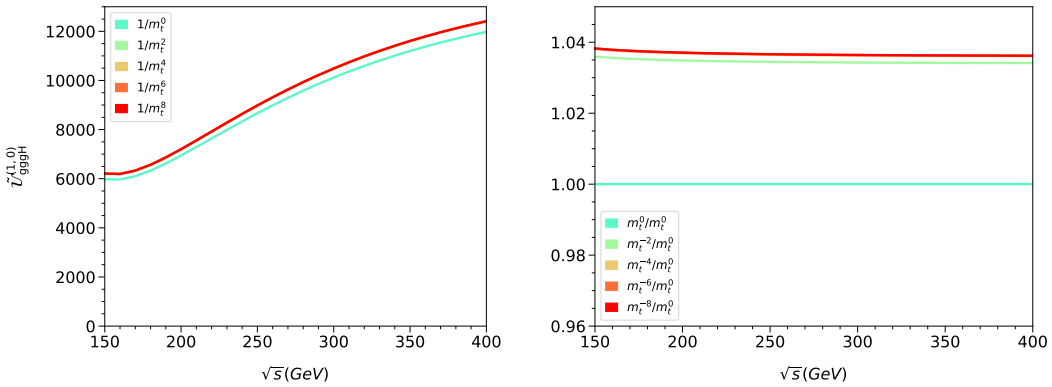

Figure 9. NLO QCD corrections to $\tilde{\mathcal{U}}_{\text{gggH}}$ as a function of $\sqrt{s}$. For the construction of the squared matrix element the infra-red subtracted form factors (eq. 6.1) have been used. The panel on the right shows the result normalized to the m_t^0 expansion term.

present results for the form factors up to order $1/m_t^{10}$ and $1/m_t^8$, respectively. We discuss the renormalization procedure in detail and compute all counterterm contributions without assuming any mass hierarchy. Thus, this part can also be applied to expansions in other kinematic limits or an exact (numerical) calculation.

Partial electroweak results for $gg \to HH$ are already available in the literature [1, 2]; in this work we provide sub-leading terms in the large-m_t expansion.

For $gg \to HH$ the expansion in $1/m_t$ does not show a convergent behaviour in the physical region $2m_H \lesssim \sqrt{s} \lesssim 2m_t$. We have demonstrated that this is due to diagrams involving a cut through a W boson and a top quark. If these diagrams are omitted, we observe reasonable convergence below $\sqrt{s} \approx 330\,\text{GeV}$. Despite the limited applicability of the large-m_t expansion we believe that our results serve as reference for future expansions in other kinematic regions or exact (numerical) calculations. Despite the convergence issues, if we assume that the order of magnitude is at least correct, in the large-m_t region the electroweak contribution provides a correction of a few tens of percent with respect to the leading order.

For the NLO electroweak corrections to $gg \to gH$ we observe very good convergence below the top quark threshold. In particular, for $\sqrt{s} < 300\,\text{GeV}$ we can provide precise predictions on the basis of an expansion which includes corrections up to $1/m_t^8$. In this region the electroweak corrections are small, below the percent level with respect to the leading order.

We also provide NLO QCD corrections for the four form factors needed for $gg \to gH$ up to $1/m_t^8$. Here a rapid convergence is also observed up to the top quark threshold.

Acknowledgments

This research was supported by the Deutsche Forschungsgemeinschaft (DFG, German Research Foundation) under grant 396021762 — TRR 257 "Particle Physics Phenomenology after the Higgs Discovery" and has received funding from the European Research Council (ERC) under the European Union's Horizon 2020 research and innovation programme grant

JHEP10(2023)033

agreement 101019620 (ERC Advanced Grant TOPUP). The work of JD was supported by the Science and Technology Facilities Council (STFC) under the Consolidated Grant ST/T00102X/1. We thank Christian Sturm for many useful discussions in connection to the renormalization of the Higgs-gluon interactions. We also thank Martin Lang for support in connection to the UFO setup of tapir. We thank Michael Spira for useful comments concerning ref. [2]. We have used the program `FeynGame` [45] to draw the Feynman diagrams.

JHEP10(2023)033

References

[1] J. Davies et al., *Higgs boson contribution to the leading two-loop Yukawa corrections to $gg \to HH$*, *JHEP* **08** (2022) 259 [arXiv:2207.02587] [INSPIRE].

[2] M. Mühlleitner, J. Schlenk and M. Spira, *Top-Yukawa-induced corrections to Higgs pair production*, *JHEP* **10** (2022) 185 [arXiv:2207.02524] [INSPIRE].

[3] S. Borowka et al., *Probing the scalar potential via double Higgs boson production at hadron colliders*, *JHEP* **04** (2019) 016 [arXiv:1811.12366] [INSPIRE].

[4] S. Dawson, S. Dittmaier and M. Spira, *Neutral Higgs boson pair production at hadron colliders: QCD corrections*, *Phys. Rev. D* **58** (1998) 115012 [hep-ph/9805244] [INSPIRE].

[5] J. Grigo, J. Hoff, K. Melnikov and M. Steinhauser, *On the Higgs boson pair production at the LHC*, *Nucl. Phys. B* **875** (2013) 1 [arXiv:1305.7340] [INSPIRE].

[6] G. Degrassi, P.P. Giardino and R. Gröber, *On the two-loop virtual QCD corrections to Higgs boson pair production in the Standard Model*, *Eur. Phys. J. C* **76** (2016) 411 [arXiv:1603.00385] [INSPIRE].

[7] T. Neumann and C. Williams, *The Higgs boson at high p_T*, *Phys. Rev. D* **95** (2017) 014004 [arXiv:1609.00367] [INSPIRE].

[8] K. Melnikov, L. Tancredi and C. Wever, *Two-loop $gg \to Hg$ amplitude mediated by a nearly massless quark*, *JHEP* **11** (2016) 104 [arXiv:1610.03747] [INSPIRE].

[9] K. Kudashkin, K. Melnikov and C. Wever, *Two-loop amplitudes for processes $gg \to Hg, qg \to Hq$ and $q\bar{q} \to Hg$ at large Higgs transverse momentum*, *JHEP* **02** (2018) 135 [arXiv:1712.06549] [INSPIRE].

[10] J.M. Lindert, K. Kudashkin, K. Melnikov and C. Wever, *Higgs bosons with large transverse momentum at the LHC*, *Phys. Lett. B* **782** (2018) 210 [arXiv:1801.08226] [INSPIRE].

[11] S.P. Jones, M. Kerner and G. Luisoni, *Next-to-leading-order QCD corrections to Higgs boson plus jet production with full top-quark mass dependence*, *Phys. Rev. Lett.* **120** (2018) 162001 [*Erratum ibid.* **128** (2022) 059901] [arXiv:1802.00349] [INSPIRE].

[12] X. Chen et al., *Top-quark mass effects in H + jet and $H + 2$ jets production*, *JHEP* **03** (2022) 096 [arXiv:2110.06953] [INSPIRE].

[13] R. Bonciani et al., *Next-to-leading-order QCD corrections to Higgs production in association with a jet*, *Phys. Lett. B* **843** (2023) 137995 [arXiv:2206.10490] [INSPIRE].

[14] R. Boughezal et al., *Higgs boson production in association with a jet at next-to-next-to-leading order in perturbative QCD*, *JHEP* **06** (2013) 072 [arXiv:1302.6216] [INSPIRE].

[15] X. Chen, T. Gehrmann, E.W.N. Glover and M. Jaquier, *Precise QCD predictions for the production of Higgs + jet final states*, *Phys. Lett. B* **740** (2015) 147 [arXiv:1408.5325] [INSPIRE].

[16] R. Boughezal et al., *Higgs boson production in association with a jet at next-to-next-to-leading order*, *Phys. Rev. Lett.* **115** (2015) 082003 [arXiv:1504.07922] [INSPIRE].

[17] X. Chen et al., *NNLO QCD corrections to Higgs boson production at large transverse momentum*, *JHEP* **10** (2016) 066 [arXiv:1607.08817] [INSPIRE].

[18] T. Gehrmann et al., *Two-loop helicity amplitudes for H + jet production to higher orders in the dimensional regulator*, *JHEP* **04** (2023) 016 [arXiv:2301.10849] [INSPIRE].

[19] M. Bonetti, E. Panzer, V.A. Smirnov and L. Tancredi, *Two-loop mixed QCD-EW corrections to $gg \to Hg$*, *JHEP* **11** (2020) 045 [arXiv:2007.09813] [INSPIRE].

[20] J. Gao et al., *Probing the Higgs boson trilinear self-coupling through Higgs boson+jet production*, *Phys. Rev. D* **107** (2023) 115017 [arXiv:2302.04160] [INSPIRE].

[21] J. Davies et al., *Double Higgs boson production at NLO: combining the exact numerical result and high-energy expansion*, *JHEP* **11** (2019) 024 [arXiv:1907.06408] [INSPIRE].

[22] L. Bellafronte et al., *Gluon fusion production at NLO: merging the transverse momentum and the high-energy expansions*, *JHEP* **07** (2022) 069 [arXiv:2202.12157] [INSPIRE].

[23] J. Davies, G. Mishima, K. Schönwald and M. Steinhauser, *Analytic approximations of $2 \to 2$ processes with massive internal particles*, *JHEP* **06** (2023) 063 [arXiv:2302.01356] [INSPIRE].

[24] *TTP*23-029 *Next-to-leading order electroweak corrections to $gg \to HH$ and $gg \to gH$ in the large-m_t limit*, .

[25] E.W.N. Glover and J.J. van der Bij, *Higgs boson pair production via gluon fusion*, *Nucl. Phys. B* **309** (1988) 282 [INSPIRE].

[26] T. Plehn, M. Spira and P.M. Zerwas, *Pair production of neutral Higgs particles in gluon-gluon collisions*, *Nucl. Phys. B* **479** (1996) 46 [*Erratum ibid.* **531** (1998) 655] [hep-ph/9603205] [INSPIRE].

[27] P. Nogueira, *Automatic Feynman graph generation*, *J. Comput. Phys.* **105** (1993) 279 [INSPIRE].

[28] M. Gerlach, F. Herren and M. Lang, *tapir: a tool for topologies, amplitudes, partial fraction decomposition and input for reductions*, *Comput. Phys. Commun.* **282** (2023) 108544 [arXiv:2201.05618] [INSPIRE].

[29] L. Darmé et al., *UFO* 2.0*: the "Universal Feynman Output" format*, *Eur. Phys. J. C* **83** (2023) 631 [arXiv:2304.09883] [INSPIRE].

[30] B. Ruijl, T. Ueda and J. Vermaseren, *FORM version* 4.2, arXiv:1707.06453 [INSPIRE].

[31] R. Harlander, T. Seidensticker and M. Steinhauser, *Complete corrections of $O(\alpha\alpha_s)$ to the decay of the Z boson into bottom quarks*, *Phys. Lett. B* **426** (1998) 125 [hep-ph/9712228] [INSPIRE].

JHEP10(2023)033

[32] T. Seidensticker, *Automatic application of successive asymptotic expansions of Feynman diagrams*, in the proceedings of the 6th *international workshop on new computing techniques in physics research: software engineering, artificial intelligence neural nets, genetic algorithms, symbolic algebra, automatic calculation*, (1999) [hep-ph/9905298] [INSPIRE].

[33] V.A. Smirnov, *Simplifying the large mass expansion*, arXiv:2307.00387 [INSPIRE].

[34] R.K. Ellis and G. Zanderighi, *Scalar one-loop integrals for QCD*, *JHEP* **02** (2008) 002 [arXiv:0712.1851] [INSPIRE].

[35] G. 't Hooft and M.J.G. Veltman, *Scalar one loop integrals*, *Nucl. Phys. B* **153** (1979) 365 [INSPIRE].

[36] V.A. Smirnov, *Some recent results on evaluating Feynman integrals*, *Nucl. Phys. B Proc. Suppl.* **157** (2006) 131 [hep-ph/0601268] [INSPIRE].

[37] M. Steinhauser, *MATAD: a program package for the computation of MAssive TADpoles*, *Comput. Phys. Commun.* **134** (2001) 335 [hep-ph/0009029] [INSPIRE].

[38] R.N. Lee, *LiteRed* 1.4*: a powerful tool for reduction of multiloop integrals*, *J. Phys. Conf. Ser.* **523** (2014) 012059 [arXiv:1310.1145] [INSPIRE].

[39] A. Denner, *Techniques for calculation of electroweak radiative corrections at the one loop level and results for W physics at LEP-200*, *Fortsch. Phys.* **41** (1993) 307 [arXiv:0709.1075] [INSPIRE].

[40] A. Denner and S. Dittmaier, *Electroweak radiative corrections for collider physics*, *Phys. Rept.* **864** (2020) 1 [arXiv:1912.06823] [INSPIRE].

[41] J. Fleischer and F. Jegerlehner, *Radiative corrections to Higgs decays in the extended Weinberg-Salam model*, *Phys. Rev. D* **23** (1981) 2001 [INSPIRE].

[42] S. Dittmaier and H. Rzehak, *Electroweak renormalization based on gauge-invariant vacuum expectation values of non-linear Higgs representations. Part I. Standard Model*, *JHEP* **05** (2022) 125 [arXiv:2203.07236] [INSPIRE].

[43] H.H. Patel, *Package-X* 2.0*: a Mathematica package for the analytic calculation of one-loop integrals*, *Comput. Phys. Commun.* **218** (2017) 66 [arXiv:1612.00009] [INSPIRE].

[44] S. Catani, *The singular behavior of QCD amplitudes at two loop order*, *Phys. Lett. B* **427** (1998) 161 [hep-ph/9802439] [INSPIRE].

[45] R.V. Harlander, S.Y. Klein and M. Lipp, *FeynGame*, *Comput. Phys. Commun.* **256** (2020) 107465 [arXiv:2003.00896] [INSPIRE].

JHEP10(2023)033